Three phase Z-source inverter with low harmonic control for G2V and V2G applications

[1]Kajal Ramesh Upare (PG Scholar), Ballarpur Institute of technology, Bamni , Tah-Ballarpur, Dist- Chandrapur email id: kajalupare1999@gmail.com

[2]Prajakta kasulkar (Asst. Prof.), Ballarpur Institute of technology, Bamni , Tah-Ballarpur, Dist- Chandrapur email id: prajuvinchurkar@gmail.com

Abstract—

The smart grid and electric vehicles (EVs) are widely used all over the world. As the key role, the Vehicle-to-Grid (V2G) has been attracting increasing attention. The bidirectional grid-connected AC/DC converter is one of the indispensable parts in the V2G system, which can realize bidirectional power flow and meet the power quality requirements for grid. A three-phase bidirectional grid-connected Z-source AC/DC converter is presented in this paper for V2G systems. It can be used to achieve the bidirectional power flow between EVs and grid, supply reactive power compensation, and smooth the power grid fluctuation. Firstly, the configuration of V2G systems is introduced, and the mathematical model of the Z-source AC/DC converter is built and for bidirectional AC/DC converters, the grid voltage feedforward decoupling scheme is applied, and the analysis of PI control strategy is proposed and the controller is designed. The system simulation model is established based on MATLAB/Simulink. Simulation results are shown, and the results evaluate the effectiveness of the model and the performance of the applied control strategy.

Keywords: V2G, G2V, EV, Z-source AC/DC converter, MATLAB Simulink

I. INTRODUCTION

Recently, with the environmental degradation, climate change, and the shortage of fossil energy, the traditional energy costs have risen a lot. Thus, it is urgent to use new and clean energy worldwide. Plug-in Electric Vehicles (PEVs) and Electric Vehicles (EVs) have attracted increasing attention worldwide [1–3], due to the representativeness of new energy vehicles. There are a lot of advantages about EVs and PEVs, such as peak power regulating, peak load shifting, environment protection, low cost, and so on. EVs and PEVs not only can be loads in grid-to-vehicle (G2V) charge mode but also can be generators in vehicle-to-grid (V2G) discharge mode [4]. Generally, both V2G and G2V applications are suitable for “V2G.”

The power converter is unidirectional for G2V in general, which includes conventional and fast charging system. Owing to the fact that the power of typical electrical vehicles is twice higher than the average household load, the grid network will be stressed by the fast charging [5]. If the G2V charger does not employ the state-of-the-art conversion, this may lead to disturbances in grid, such as undesirable peak loads, harmonics, and low power factor [6, 7]. Thus, it is essential to support energy injection back to the grid in V2G system. Bidirectional grid-connected AC/DC converter is one of the indispensable parts in the V2G system, which can realize the sinusoidal input current and bidirectional power flow. For V2G applications, improving power density, reducing input and output current ripple, and having reactive power compensation capability are the major research directions for bidirectional AC/DC converter [8–10].

In recent years, there are different kinds of AC/DC converter topologies used in the V2G system, including single-stage single-phase and three-phase, two-stage single-phase and three-phase, ZVS inverter, and so on [11, 12]. Reference [13] presents an electrical vehicle charger that used a single-phase interleaved AC/DC boost converter. In[14], a high-performance single-phase bridgeless interleaved PFC converter is proposed. Both [13, 14] have the same function, which can reduce the battery charge and discharge current ripple, however, neither of them could work with wide output voltage. In [15, 16], unidirectional buck-boost converters with wide output voltage are proposed, which can reduce the Total Harmonic Distortion (THD) of AC current. Because of the unidirectional switches, all these converters cannot feedback the battery energy to the grid. To realize the bidirectional power flow, the AC/DC matrix converters are proposed in [17]. However, the converter is known for its large amounts of semiconductor switches and high-frequency operation, which will lead to higher cost and larger losses including switching losses and conduction losses. In some advanced control logic for three-phase Z-source converters has been proposed to achieve better dynamic performance, realize ZVS rectifying, reduce grid current distortion, decouple active and reactive power and increase voltage conversion ratio. However, these control methods require tremendous and complicated calculations to meet the special requirements of designated applications with more passive devices added. Those control schemes are often complicated.

In this paper, three new modulation schemes of inserting shoot-through states are proposed. Among them, sine variable modulation shows better performance over harmonic suppression and is therefore further developed into a closed-loop control method. The converter could be connected to the grid or a three-phase load. The switch S1 and circuit breaker S2 determine the working mode. To simplify the calculation, the input DC voltage source is divided into two voltage sources, each has the magnitude of Vdc/2, and the middle point is labelled as O. Compared to conventional control schemes, the proposed method in this paper has the following advantages: low harmonics in output voltage and current; support of bidirectional operation; easy to implement without complicated algorithm or computation burden; easy to modify for the control in grid-connected mode. [18], a current-source rectifier is shown with an auxiliary switching network. The advantages of this converter are high efficiency and achieved the bidirectional power flow, but it will reduce the battery life owing to the input current ripple. The study in [19] proposed a current-source rectifier with PWM pulse signal trilogy control method. In [20, 21], the intelligence protection technique is proposed, which can be used in the high-power grid-connected converter. The authors of presented the maximum current control and grid voltage full-feedforward scheme for three-phase voltage-source rectifier.

There are several different disadvantages in the topologies mentioned above when used in V2G, such as the narrow output voltage range, large losses, and high input current ripple. As an effective alternative, a three-phase bidirectional grid-connected converter for V2G system is analysed and designed in this paper, which realized bidirectional power flow, high efficiency, unity power factor, and wide battery pack voltage range. In Section 2, the system configuration is introduced, and the mathematical models of bidirectional AC/DC and DC/DC converter are built in detail. In Section 3, the control strategies, including the grid voltage feedforward decoupling scheme, and the double closed-loop control of AC/DC converter are analysed and designed. In Section 4, the simulation results are proposed and discussed. Finally, conclusions of this paper are in Section 5.

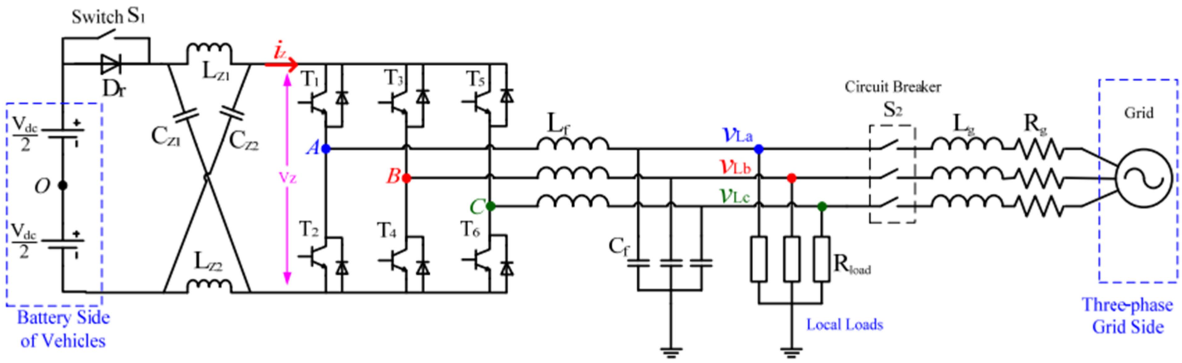

Fig.1 Topology of a bi-directional three-phase Z-source converter

II. THREE PHASE Z-SOURCE INVERTER WORKING

The analysis of Z-source based multilevel inverter is examined by using Matlab/Simulink in [9]. The performances of the ZSI are compared with the other traditional inverter topologies. As a result, the increasing in the voltage and current are filtered by the capacitors and inductors of the ZSI. Authors in [10] propose a single stage ZSI topology which eliminates some drawbacks of the conventional inverters like being the less or more output AC voltage than the input DC voltage and the shoot through faulty by providing two switches of the same leg to be gated in the circuit. Since ZSI also eliminates the dead time in the circuit, distortion is reduced and reliability of the system increases. In this study, the performance of ZSI is examined about reducing THD by using Matlab/Simulink for different load situations and modulation indexes. It is observed from the simulation results that ZSI shows higher performance than conventional VSI and ZSI. In the paper [11] explains a single stage ZSI topology based on the duty ratio and modulation index. The simulation of a single-phase induction motor is realized by the control of the single phase ZSI. This inverter provides lower line harmonics and shoot-through duty cycle. Therefore, it increases the reliability and efficiency and also extends the output AC voltage range of the inverter. [12] presents a ZSI concept which can also be used to DC-DC, AC-DC and AC-AC power conversions. A different impedance circuit is used to combine the source and power circuit. By a simple boost control method, Matlab/Simulink simulation and analysis of the ZSI are carried out in this study. The triggering pulses for six switches of the three phase ZSI are applied in the simulations. The simulation results show that the desired load sinusoidal voltage and current are obtained by the filtered ZSI compared to the traditional inverters. In [13], a topology of two level ZSI is explained. Two level ZSI receives the power supply from the PV. Sinusoidal Pulse Width Modulation (SPWM) is used to control the switches of the ZSI for the shoot through and non-shoot through operation modes. This inverter provides high efficiency, low cost, and low leakage current for the PV systems. Simulation and design of the single phase ZSI are given in [14, 15]. ZSI eliminates the limitations of the traditional VSI and CSI and presents a novel power conversion concept. By using SBC PWM technique, the simulation of ZSI is realized for various modulation indexes. As a result, it is observed that the sinusoidal load voltage and current can be obtained by the filtered ZSI compared to the conventional inverters.

Three phase ZSI topology includes R-L output filter and loads as illustrated in Fig. 1. The equivalent circuit of the ZSI is shown in Fig. 2 [16]. In this structure, there is a single type of impedance circuit consisting of two capacitors and two inductors connected in an X-shape. This structure allows the main circuit to be transferred to the load, power supply or other converter. In this way, the circuit structure of traditional inverters using capacitors and inductors turns into a unique new circuit structure. In this circuit, when the inductances L1 and L2 and capacitances C1 and C2 are the same values, the Z source network becomes symmetrical.

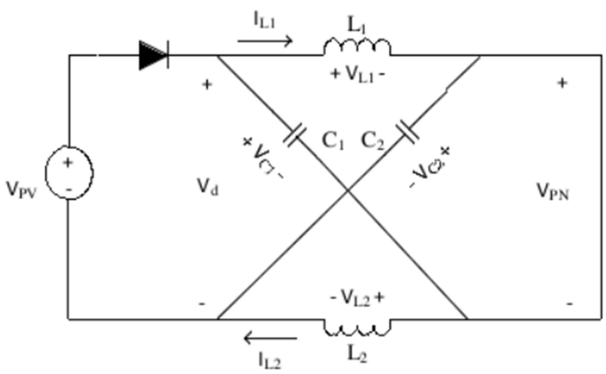

Figure 2. Equivalent circuit of the ZSI

As seen from the Fig. 2, the voltages can be written as follows

$$V_{C1} = V_{C2} = V_C \quad (1)$$

$$\upsilon_{L1} = \upsilon_{L2} = \upsilon_L \quad (2)$$

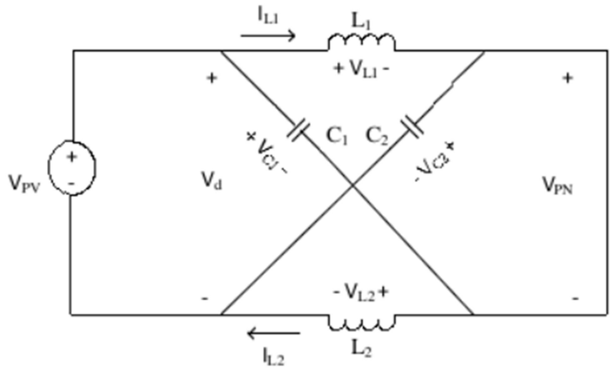

Figure 3. Equivalent circuit of the ZSI with non-shoot through state

According to the Fig. 3, the voltages in the circuit are given by

$$\upsilon_L = V_{PV} - V_C \quad (3)$$

$$\upsilon_d = V_{PV} \quad (4)$$

$$\upsilon_{PN} = V_C - \upsilon_L = 2V_C - V_{PV} \quad (5)$$

In the shoot-through situation (T1), the Z-source circuit is shown by a short-circuit in the Fig. 4.

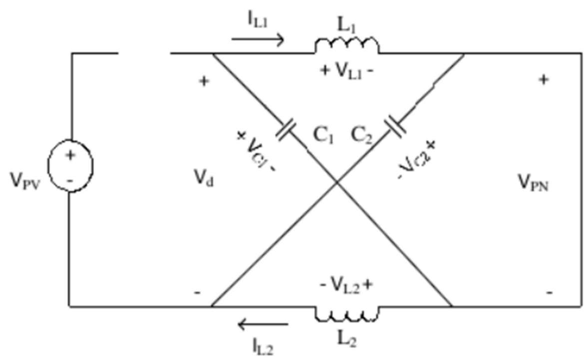

Figure 4. Equivalent circuit of the ZSI when the inverter is in the shoot through state

As seen from the Fig. 4, the voltages are calculated by using Kirchhoff's voltage law as follows

$$\upsilon_L = V_C \quad (6)$$

$$\upsilon_d = 2V_C \quad (7)$$

$$\upsilon_{PN} = 0 \quad (8)$$

III. CONTROL STRUCTURE

Three sinusoidal modulating signals at the frequency of the desired output but displaced from each other by 2π/3 phase are generated. The triangular carrier wave is compared with the modulation waves to generate six gate signals [17]. The concept is modifying the magnitude of three modulation waves to create overlaps. In Fig. 5(a), the sine modulation waves of generating signals for switch T1 and T2 in phase A bridge are presented. The black solid curve represents a standard sine wave whose magnitude ranges from –M to M, where 0 < M < 1. Two more modulation waveforms are derived by adding a variable b(t) which varies with time respectively. The red dashed modulation wave is used for generating gate signals for upper switch T1, which is marked as wT1 [18]. The blue dotted modulation wave is used for generating gate signals for lower switch T2, which is marked as wT2. Fig. 5(b) is a zoomed view of the circled part of Fig. 5(a). It shows the overlap of switching signals GT1 and GT2 by two different modulation waves. For simplicity, b(t) is set as a constant in Fig. 5.

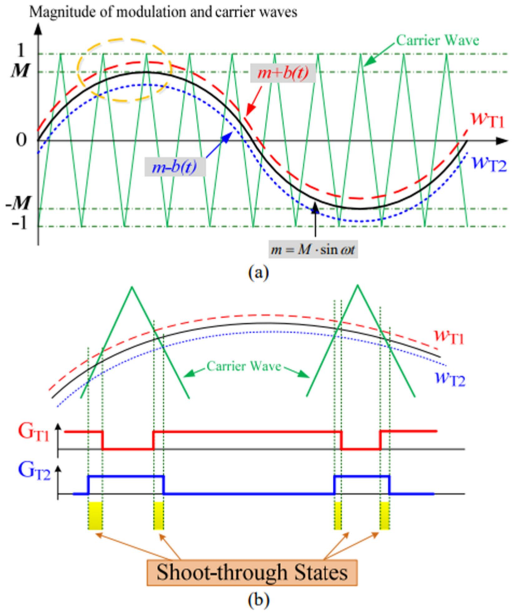

Fig.5: Shoot-through states inserting by overlap: (a) Modulation waves in one cycle; (b) Zoomed view

$$\begin{cases} m_A = M \cdot \sin \omega t \\ m_B = M \cdot \sin(\omega t - \frac{2}{3}\pi) \\ m_C = M \cdot \sin(\omega t - \frac{4}{3}\pi) \end{cases} \quad (9)$$

The magnitudes of three modulation waves for each bridge are shown in (4), where M represents the magnitude of sine modulation waves; and mA, mB and mC represent the instantaneous magnitude of modulation waves of phase A, B and C [19] [20]. Both mA, mB and mC range from –M to M. The three modulation waves are compared to the carrier waves in Fig. 5(b), then six pulsed gate signals are generated accordingly as shown in Fig. 6.

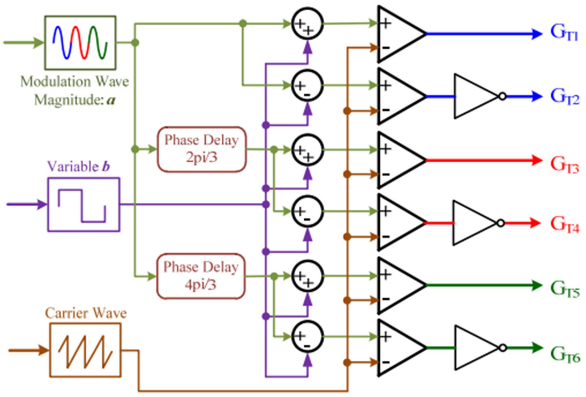

Fig.6: Generation of switching signals to insert shoot-through states

$$\begin{cases} m_{Au} = M \cdot \sin \omega t + b_1(t) \\ m_{Bu} = M \cdot \sin(\omega t - \frac{2}{3}\pi) + b_3(t) \\ m_{Cu} = M \cdot \sin(\omega t - \frac{4}{3}\pi) + b_5(t) \\ m_{Al} = M \cdot \sin \omega t + b_2(t) \\ m_{Bl} = M \cdot \sin(\omega t - \frac{2}{3}\pi) + b_4(t) \\ m_{Cl} = M \cdot \sin(\omega t - \frac{4}{3}\pi) + b_6(t) \end{cases} \tag{10}$$

The magnitude variation of each modulation wave is marked as a function bn(t), where n represents the serial number of switches. The modified magnitudes of modulation waves are given in (5), where mAu, mBu and mCu represent the instantaneous magnitudes of modulation waves used for generating pulse signals for the upper switches of phase A, B and C, and mAl, mBl and mCl represent the instantaneous magnitude of modulation waves used for generating pulse signals for the lower switches of phase A, B and C [21].

IV. SIMULATION RESULTS

An 80 kW V2G system simulation model is established in MATLAB/Simulink. The control schemes mentioned above are applied to the AC/DC converter. And the single current closed loop is used in bidirectional DC/DC converter. System configuration is shown in Figure 1, and the detailed parameters of the converter are shown in Table 1.

Table 1: System parameters.

Symbol	Parameters	Value (V)
e_a e_b e_c	Grid voltage (RMS)	220
L	Grid-side filter inductance	0.9
R	Resistor	0.1
C	DC-bus filter capacitor	12000
L_1	DC inductance	0.2
C_o	DC capacitor	2000
u_{dc}	DC-bus voltage	800
u_{bat}	Battery voltage	500
f_s	Switching frequency	10
f_{line}	Grid frequency	50

Figure 7 shows the converter output DC voltage waveforms with zero load. The initial voltage of converter is 570 V, and the output reference voltage is 800 V. After about 0.1 s, the output voltage is 800 V. The overshoot voltage of system is about 20 V, and the output ripple voltage is about 1 V. Figure 8 shows the dynamic performance of three-phase bidirectional grid-connected converter. The load steps from 0 to full load, when time 0.01s.

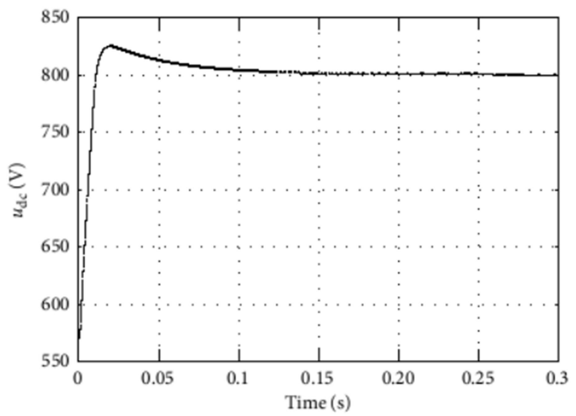

Figure 7: The DC bus voltage waveform of AC/DC converter without load.

From Figure 8(a), udc drops from 800V to 747.1 V at time = 0.01 s. Then, the voltage returns to original output, which takes about 140.2 ms, and the ripple is about 1.8 V. Grid-connected. Figure 8(b). The currents increase at time = 0.01 s and eventually stabilize at 99.77 A RMS. The Fourier analysis of grid-connected current shows that THD of the grid current is about 2.3%.Through comparing udc and ia, ib, ic in Figure 8, it can be concluded that the proposed AC/DC converter works with a balanced and low THD three-phase grid-connected current, and it performs fast DC voltage regulation under full load disturbances.

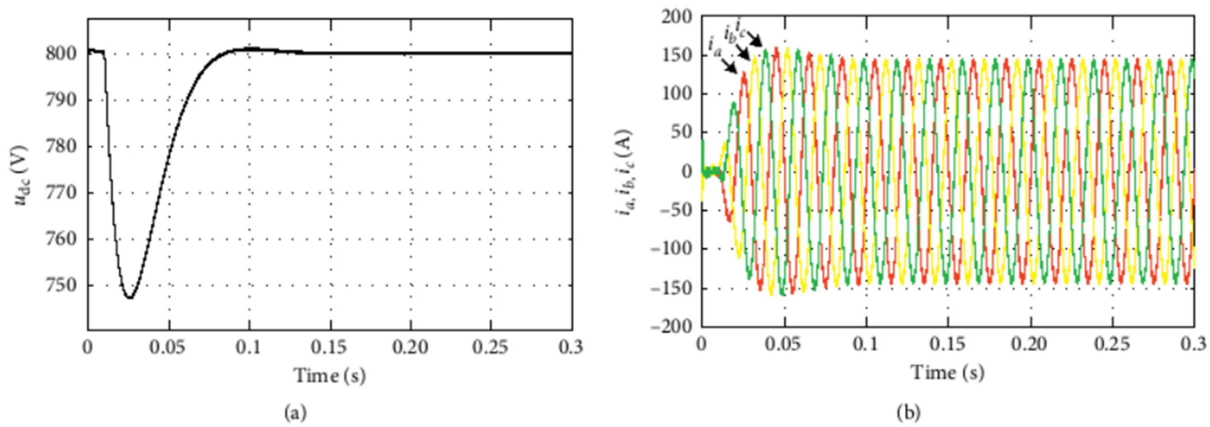

Figure 8: Step response of converter. (a) The step response of AC/DC converter DC bus voltage. (b) The step response of AC/DC converter grid-connected current.

Figure 9 shows the simulation results of the V2G system in charging and discharging. From time 0 s to time 0.25 s, the power flow of the system is negative, which indicates that the battery is discharging. From time 0.25 s to time 0.5 s, the power flow is positive, which indicates that the battery is charging. And the power of charge and discharge is 80 kW. From Figure 9(a), udc increases from 800 V to 837.6 V at the beginning of discharging. After about 175.37 ms, udc restored to original output and the ripple is about 2 V. udc drops from 800 V to 722.5 V, when the power flow changes at time = 0.25 s. After about 200.25 ms, the voltage restored to original output. Figure 9(b) shows the battery State of Charge (SOC). From time = 0 s to time = 0.25 s, the battery is discharging. After time = 0.25 s, the battery is charging. Figures 9(c) and 9(d) depict the phase A grid-connected current and voltage. It can be observed that ia and ea are the same frequency but opposite phase, when time 0.25 s. And ia and ea are the same frequency and phase, when time > the current THD is 3.5%, while the battery is discharging. And the current THD is 2.23%, while the battery is charging.

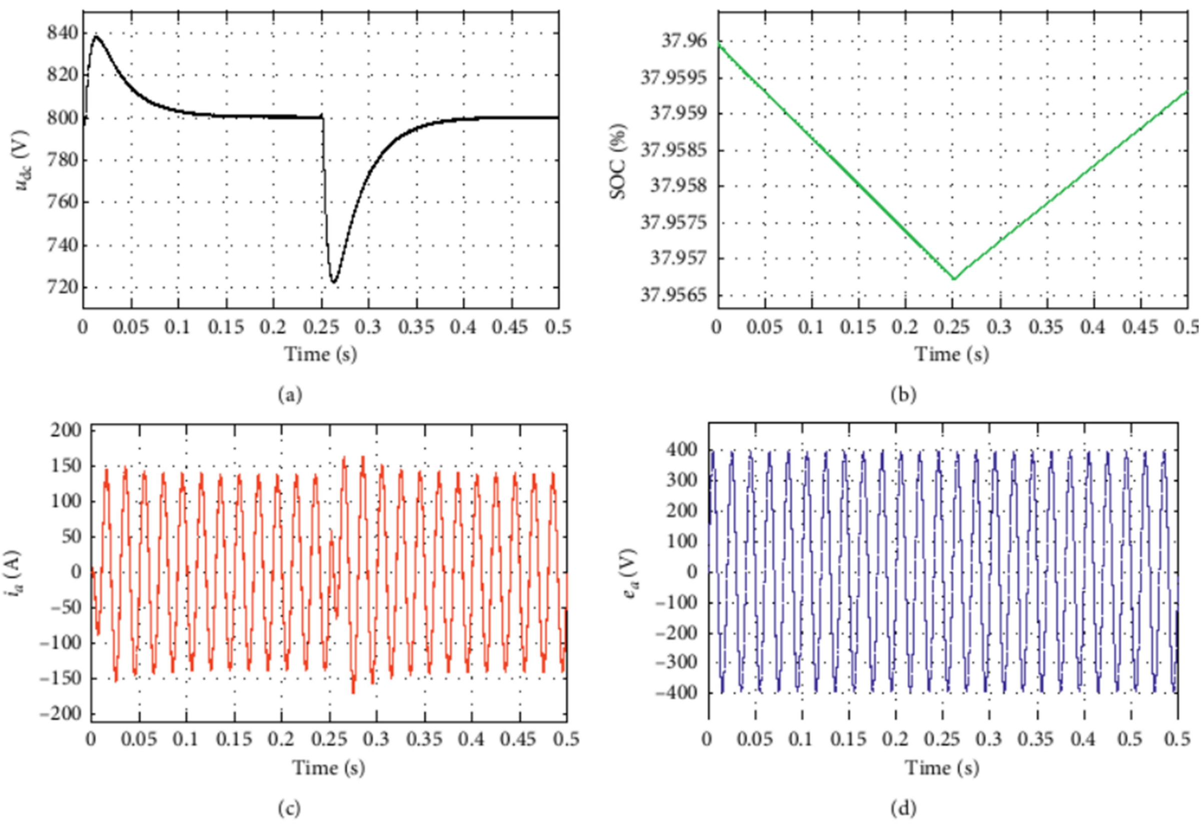

Figure 9: The waveforms of V2G system in different conditions. (a) The DC bus voltage of bidirectional AC/DC converter. (b) The state of charge (SOC) of battery. (c) The gird-connected current curve of phase A. (d) The grid voltage curve of phase A.the simulation results show the correctness of design in terms of high-power factor, low current harmonic distortion, and constant output voltage.

V. CONCLUSION

A three-phase bidirectional grid-connected AC/DC converter for V2G system is presented in this paper. And the mathematic model of three-phase AC/DC converter in the synchronous d − q frame is built. Since the grid current will be affected by the grid voltage distortion and the cross-coupling terms, the feedforward scheme of grid voltage is applied to the bidirectional AC/DC converter in the synchronous d − q frame. And the PI controllers of voltage and current closed loop for the converter are designed. Finally, the model is established in MATLAB/Simulink. Simulation results show that the converter works well for V2G application with unity power factor, low voltage ripple, high efficiency, and low current THD.

REFERENCES

[1] S. Habib, M. M. Khan, F. Abbas, L. Sang, M. U. Shahid, andH. Tang, “A comprehensive study of implemented international standards, technical challenges, impacts and prospects for electric vehicles,” IEEE Access, vol. 6, pp. 13866–13890, 2018.

[2] S. Esther, S. K. Singh, A. K. Goswami et al., "Recent challenges in vehicle to grid integrated renewable energy system: a review," in Proceedings of the 2018 Second International Conference on Intelligent Computing and Control Systems (ICICCS), pp. 427–435, Madurai, India, 2018.

[3] P. K. Joseph, E. Devaraj, and A. Gopal, "Overview of wireless charging and vehicle-to-grid integration of electric vehicles using renewable energy for sustainable transportation," IET Power Electronics, vol. 12, no. 4, pp. 627–638, 2019.

[4] M. A. Masrur, A. G. Skowronska, J. Hancock et al., "Military-based vehicle-to-grid and vehicle-to-vehicle microgrid-system Architecture and implementation," IEEE Transactions on Transportation Electrification, vol. 4, no. 1, pp. 157–171, 2018.

[5] B. Sah, P. Kumar, R. Rayudu, S. K. Bose, and K. P. Inala, "Impact of sampling in the operation of vehicle to grid and its mitigation," IEEE Transactions on Industrial Informatics, vol. 15, no. 7, pp. 3923–3933, 2019.

[6] T. Chen, X.-P. Zhang, J. Wang et al., "A review on electric vehicle charging infrastructure development in the UK," Journal of Modern Power Systems and Clean Energy, vol. 8, no. 2, pp. 193–205, 2020.

[7] S. I. Vagropoulos, G. A. Balaskas, and A. G. Bakirtzis, "An investigation of plug-in electric vehicle charging impact on power systems scheduling and energy costs," IEEE Transactions on Power Systems, vol. 32, no. 3, pp. 1902–1912, 2017.

[8] A. Sridhar and A. R. Prabu, Bidirectional AC-DC Converter for Vehicle-To-Grid (V2G) Applications, Marquette University, Milwaukee, WI, USA, 2015.

[9] S. Liu, D. Xin, and L. Yang, "A novel single-phase bidirectional electric-drive-reconstructed onboard converter for electric vehicles," IEEE Access, vol. 8, pp. 44739–44747, 2020.

[10] J. Zhang, H. Yan, N. Ding et al., "Electric vehicle charging network development characteristics and policy suggestions," in Proceedings of the 2018 International Symposium on Computer, Consumer and Control (IS3C), pp. 469–472, Taichung, China, 2018.

[11] B. Koushki, P. Jain, and A. Bakhshai, "Topology and controller of an isolated bi-directional AC-DC converter for electric vehicle," in Proceedings of the 2016 IEEE Energy Conversion Congress and Exposition (ECCE), pp. 1–8, Milwaukee, WI, USA, 2016.

[12] K. V. Sing, H. O. Bansal, and D. Singh, "A comprehensive review on hybrid electric vehicles: architectures and components," Journal of Modern Transportation, vol. 27, no. 2, pp. 77–107, 2019.

[13] P. Yang, T. Peng, H. Wang et al., "A single-phase current-source bidirectional converter for V2G application," in Proceedings of the 2017 IEEE 3rd International Future Energy Electronics Conference and ECCE Asia (IFEEC 2017-ECCE Asia), pp. 704–709, Kaohsiung, Taiwan, 2017.

[14] A. K. Singh and M. K. Pathak, "Single-phase bidirectional ac/ dc converter for plug-in electric vehicles with reduced conduction losses," IET Power Electronics, vol. 11, no. 1, pp. 140–148, 2018.

[15] B. Singh and R. Kushwaha, "A PFC based EV battery charger using a bridgeless isolated SEPIC converter," IEEE Transactions on Industry Applications, vol. 56, no. 1, pp. 477–487, 2020.

[16] M. R. T. Hossain, A. H. Abedin, and M. A. Choudhury, "A single phase SEPIC AC-DC Converter with improved power factor and input current THD," in Proceedings of the 2016 9th International Conference on Electrical and Computer Engineering (ICECE), pp. 373–376, Dhaka, Bangaladesh, 2016.

[17] T.-L. Nguyen and H.-H. Lee, "An enhanced control strategy for AC-DC matrix converters under unbalanced grid voltage," IEEE Transactions on Industrial Electronics, vol. 67, no. 3, pp. 1718–1727, 2020.

[18] D. Mishra, B. Singh, and B. K. Panigrahi, "Adaptive current control for a Bi-directional interleaved EV charger with disturbance rejection," in Proceedings of the 2020 IEEE International Conference on Power Electronics, Smart Grid and Renewable Energy (PESGRE2020), Cochin, India, pp. 1–6, 2020.

[19] J. Zhao and Q. Jiang, "Research on a new control strategy for three-phase current-source PWM rectifier," in Proceedings of the 2017 Eighth International Conference on Intelligent Control and Information Processing (ICICIP), pp. 157–161, Hangzhou, China, 2017.

[20] O. Noureldeen, I. Hamdan, and B. Hassanin, "Design of advanced artificial intelligence protection technique based on low voltage ride-through grid code for large-scale wind farm generators: a case study in Egypt," SN Applied Sciences, vol. 1, no. 6, pp. 1–19, 2019.

[21] O. Noureldeen and I. Hamdan, "Design of robust intelligent protection technique for large-scale grid-connected wind farm," Protection and Control of Modern Power Systems, vol. 3, no. 1, pp. 1–13, 2018.